The Reductive Elimination of Methane from ansa-Hydrido(methyl)metallocenes of Molybdenum and Tungsten: Application of Hammond's Postulate to Two-State Reactions

José-Luis Carreón-Macedo, Jeremy Harvey, Rinaldo Poli

The Reductive Elimination of Methane from *ansa*-Hydrido(methyl)metallocenes of Molybdenum and Tungsten: Application of Hammond's Postulate to Two-State Reactions

José-Luis Carreón-Macedo,[a] Jeremy N. Harvey,*[a] and Rinaldo Poli*[b]

[a]*School of Chemistry, University of Bristol, Cantock's Close, Bristol BS8 1TS, U.K.*

[b]*Laboratoire de Chimie de Coordination, CNRS, 205 Route de Narbonne, 31077 Toulouse cedex, France*

Proofs to:

Rinaldo Poli

Tel +33-561333195, +33-562885863

Fax +33-561553003

E-mail poli@lcc-toulouse.fr

Keywords: Density Functional Theory, Metallocenes, Minimum Energy Crossing Points, Hammond's Postulate, Spin Crossover Reactivity

Abstract

The energetic profile of the methane reductive elimination from a selected number of methylhydrido molybdenocene and tungstenocene derivatives has been calculated by DFT methods. The calculations were carried out for the $CH_2(C_5H_4)_2M$ (***a*-M**), $SiH_2(C_5H_4)_2M$ (**a-H_2Si-M**), and $SiMe_2(C_5Me_4)_2M$ (**a-Me_2Si-M***) *ansa*-metallocene systems for M = Mo, W. They include the full optimization of minima (the methylhydrido starting complexes, **M(H)(CH_3)**, the intermediate methane complexes, **M(CH_4)**, and the metallocene products in the singlet and triplet configurations, **^{3}M** and **^{1}M**), transition states (for the methyl hydride reductive elimination, **M-TS_{ins}**, and for the hydrogen exchange, **M-TS_{exch}**), and the minimum energy crossing point (**M-MECP**) leading from the singlet methane complexes to the corresponding triplet metallocenes. The results are compared with those previously obtained for the simpler $(C_5H_5)_2M$ (**Cp_2M**) systems (J. C. Green, J. N. Harvey, and R. Poli, *J. Chem. Soc, Dalton Trans.*, 2002, 1861). The calculated energy profiles, notably the relative energies of **M-TS_{ins}** and **M-MECP**, are in agreement with available experimental observations for the **a-Me_2Si-M*** systems. The comparison of the energies and geometries of the rate determining **M-TS_{ins}** and **M-MECP** structures with those of the thermodynamically relevant minima for the various systems show the applicability of Hammond's postulate to two-state reactions. However, one notable exception serves to show that the principle is only quantitatively reliable when all the potential energy surfaces for the set of analogous reactions have similar shapes.

Introduction

The reductive elimination of alkyl hydride complexes to liberate a molecule of saturated alkane is a fundamental step in catalytic hydrogenation,[1, 2] whereas the reverse process is relevant for the functionalization of hydrocarbons.[3, 4] Both have been topics of intense investigation.[5-7] A particular class of compounds that has attracted considerable attention is the family of the Group 6 metallocenes, $Cp'_2M(H)(R)$ (M = Mo, W; Cp' = any cyclopentadienyl ligand),[8-13] in particular with R = CH_3, involving the formation and/or activation of methane. An interesting feature of this family (shared, however, with other systems) is that the 16-electron complex Cp'_2M has a different spin state – a triplet – than the diamagnetic $Cp'_2M(H)(R)$.[14-17] Thus, the process interconverting the two complexes is a two-state reaction.[18] Experimental work suggests that the elimination of methane from $Cp'_2M(H)(CH_3)$ proceeds via σ-CH_4 intermediates, $Cp'_2M(\eta^2\text{-}CH_4)$ where the CH_4 ligand coordinates via the electrons of one σ C-H bond, because scrambling processes between the hydride and the methyl H atoms have sometimes been found by deuterium labeling experiments to be competitive or faster than the elimination process. Theoretical studies have addressed this issue and confirmed the existence of such intermediates, which possess a singlet ground state like the hydridoalkyl reagent.[15, 17] In addition, these studies have identified the transition states leading to the H exchange and to the oxidative addition.

To fully understand the reaction coordinate leading to the elimination products, however, it is also necessary to explicitly determine the minimum energy crossing point (MECP) between the singlet and triplet surfaces. As shown schematically in Figure 1, crossing occurs during the elimination process of the CH_4 ligand from the coordination sphere of the intermediate σ-CH_4 complex, **M(CH_4)**, leading to the triplet metallocene, ^{3}**M**.[17] There are two possible limiting scenarios. In the first one (part *a* of Figure 1), the insertion

transition state (**M-TS$_{ins}$**) leading from the **M(CH$_4$)** intermediate to the hydridomethyl complex, **M(H)(Me)**, has a lower energy than the MECP (**M-MECP)**. When this is the case, provided the exchange of the coordinated C-H bond for the methane ligand also occurs through a lower energy transition state (**M-TS$_{exch}$**) than the **M-MECP**, the hydrogen scrambling process is faster than the methane elimination. This situation can be kinetically defined as a pre-equilibrium between the starting **M(H)(Me)** complex and the intermediate **M(CH$_4$)** complex, followed by rate limiting methane dissociation, in which the overall rate is controlled by the **M-MECP** energy. In the second scenario (part *b* of Figure 1), the energy of **M-TS$_{ins}$** is higher than the **M-MECP**. In this case, the methane elimination is kinetically a one-step process determined by the **M-TS$_{ins}$** energy, and no H scrambling is observed. In our previous computational study of this phenomenon for the simple metallocenes of Mo and W, Cp_2M,[17] which included the explicit calculation of **M-TS$_{ins}$** and **M-MECP** geometries and energies, we found that E(**M-TS$_{ins}$**) > E(**M-MECP**) for Cp_2Mo (31.0 and 4.3 kJ mol^{-1}, respectively, relative to the **M(CH$_4$)** intermediate), whereas the two energies are comparable for Cp_2W (9.8 and 9.1 kJ mol^{-1}). Thus, the Mo system corresponds to the situation (*b*) whereas the W analogue shows an intermediate behavior. Analogous calculations on the *ansa* system $[CH_2(C_5H_4)_2]W$ (**a-W**), on the other hand, resulted in situation (*a*): E(**M-TS$_{ins}$**) = 4.4 kJ mol^{-1} and E(**M-MECP**) = 17.3 kJ mol^{-1}. The corresponding Mo *ansa* system (**a-Mo**) was not explored in detail.

<Figure 1>

Recent elegant work by Parkin *et al.* has provided experimental evidence, through the determination of kinetic isotope effects (KIE), for the occurrence of these two limiting situations for the methane or benzene reductive eliminations from $[Me_2Si(C_5Me_4)_2]$-

Mo(H)(Ph) and [$Me_2Si(C_5Me_4)_2$]W(H)(R) where R = Me, Ph. Whereas the molybdenum system is characterized by a normal KIE, *i.e.* $k_H/k_D > 1$, the tungsten systems exhibit an overall inverse KIE which derives from a combination of an inverse *equilibrium* isotope effect (EIE) for the reductive elimination step, and a near-zero KIE for the spin-forbidden methane dissociation step. The KIE for the reductive elimination step is, like for the Mo case, normal, but it does not determine the overall KIE because it is not the rate-limiting step.[13] This can be expressed in other terms: the nature of the bonding of the key hydrogen (or deuterium) atom at the different stationary points along the reaction coordinate is qualitatively the same in the Mo and W cases. Bonding is fairly tight for the starting metal hydride (in the M–H or M–D bond), then becomes looser at the elimination TS, where H (D) is only partly bonded to M and C, then is at its tightest in the strong C–H (or C–D) bond which is present in the intermediate, the MECP and the products. This difference in bonding leads to differences in zero-point energy, which, together with the fact that the overall bottleneck to reaction is different in the two cases, explains the isotope effects. Thus, the normal KIE for the decomposition of the Mo complex corresponds to the situation illustrated in Figure 1(*b*), whereas the overall inverse KIE observed for the W complexes results from an energetic profile as shown in Figure 1(*a*).

This difference was attributed by Parkin *et al.* to the relative stability of the starting [$Me_2Si(C_5Me_4)_2$]M(H)(R) and final [$Me_2Si(C_5Me_4)_2$]M complexes (here represented as **a-Me_2Si-W*** or **a-Me_2Si-Mo***), implicitly invoking Hammond's principle for the relative energy of the two critical points. This hypothesis, however, was not accompanied by a computational verification. In a separate contribution, Parkin *et al.* have reported calculations of the relative energy of the TS and crossing point for the W system, the crossing point having a marginally higher energy (ca. 33 kcal mol^{-1}) than the TS (30.1 kcal mol^{-1}).[19] That study, however, does not report similar calculations for the Mo system. In addition, the crossing

point was estimated by a procedure that we have termed the "partial optimization method",[20] which is more approximate than the explicit calculation of the MECP. The purpose of the present study is to complete the comparison of the *ansa* $[CH_2(C_5H_4)_2]M$ (M = Mo, W) systems, to compare these systems with the simpler metallocenes that we have previously described,[17] and to analyze the TS and MECP energies and geometries in more details, in light of Hammond's postulate. In addition, we extend and apply the same analysis to the simplified systems $[H_2Si(C_5H_4)_2]Mo$ (**a-H_2Si-Mo**), $[H_2Si(C_5H_4)_2]W$ (**a-H_2Si-W**), and finally to the experimentally reported systems **a-Me_2Si-W*** and **a-Me_2Si-Mo***. The labels used throughout this contribution contain a first part to identify the metallocene core (the generic **M** in Figure 1), and a second part to identify the way in which this interacts with the methane molecule, following the pattern shown in Figure 1. Views of the hydridomethyl derivatives for all systems investigated in this study, and the corresponding labels, are given in the Chart.

<Chart>

Results and Discussion

1. Cp_2M and a-M systems

The new results reported here complete a previous study of ours, dealing with the reductive elimination process of CH_4 from methylhydrido derivatives of Cp'_2M, where Cp' = Cp (**Cp_2M**) or Cp'_2 = $CH_2(C_5H_4)_2$ (**a-M**) and M = Mo and W.[17] In that study, DFT calculations were carried out with the B3LYP functional and two different basis sets. The complete set of critical points along the reaction pathway (including **M-TS_{ins}** and **M-MECP**) was determined only with the simpler LANL2DZ basis set, whereas a more sophisticated basis set where the C and H atoms were described by polarized 6-31G** basis functions was

used only to recalculate all local minima. In addition, all the calculations were carried out using the standard B3LYP level of density functional theory. In recent work, we have found that relative energetics obtained for organometallic species, especially the spin-state splitting between high- and low-spin states, can depend quite strongly on the functional used. [21-23] We therefore decided to validate the method used in our previous work by considering larger basis sets and other DFT functionals, for one of the systems under consideration, i.e. $[CH_2(C_5H_4)_2]W$ (**a-W**). These results are summarized in Table 1.

Table 1. Energies (kJ mol^{-1}) relative to $^3[M]+CH_4$ of various points on the relevant singlet and triplet potential energy surfaces for the $[CH_2(C_5H_4)_2]W$ (**a-W**) system.[a]

	B3LYP			B3PW91[b]	BP86[b]
	LANL2DZ	6-31G**	SDD/6-311+G**		
^{1}**a-W** + CH_4	*35.4*	*33.4*	31.5	32.1	19.5
^{3}**a-W** + CH_4	*0.0*	*0.0*	0.0	0.0	0.0
a-W(CH_4)	*9.7*	*4.5*	5.4	–0.4	–16.9
a-W(H)(Me)	*–121.9*	*–123.3*	–118.4	–120.8	–134.5

[a] Values in italics are taken from our previous contribution.[17] [b] Single-point energies at the B3LYP/SDD,6-311++G** geometries.

As can be seen, the four sets of calculations using the B3LYP and B3PW91 hybrid functionals yield very similar results. The binding energy of the **a-W(CH_4)** intermediate is slightly lower with the small basis set, and slightly larger with the B3PW91 functional, but the differences are smaller than the expected error levels in both cases. Somewhat larger differences are noted between the hybrid functionals and the gradient-corrected BP86 functional. These differences can all be interpreted in terms of a relatively larger stabilization of the triplet fragment with the hybrid functionals than with BP86. This type of behaviour is fairly general[21] and can be attributed to the admixture of Hartree-Fock exchange in hybrid functionals which favours the high-spin state. Even here, though, the differences between methods are only of the order of 10 – 15 kJ mol^{-1}, and would be unlikely to affect the

qualitative conclusions. We have therefore carried out the rest of this work using the simpler B3LYP/LANL2DZ and B3LYP/6-31G** calculations.

In our earlier work, as well as locating some of the stationary points only with the smaller LANL2DZ basis, no TS and MECPs were calculated, with either basis, for the *ansa*-Mo system, $[CH_2(C_5H_4)_2]Mo$ (**a-Mo**). We have now completed the study of these four systems by calculating all missing TS and MECP at both levels, see Table 2.

Table 2. Energies (kJ mol^{-1}) relative to ^{3}**M**+CH_4 of various points on the relevant singlet and triplet potential energy surfaces for the **Cp$_2$M** and **a-M** (M = Mo, W) metallocenes.[a]

	M = **Cp$_2$Mo**		**M** = **Cp$_2$W**		**M** = **a-Mo**		M = **a-W**	
	LANL2DZ	6-31G**	LANL2DZ	6-31G**	LANL2DZ	6-31G**	LANL2DZ	6-31G**
^{1}**M** + CH_4	*100.9*	*96.1*	*79.8*	*81.9*	*40.6*	*33.9*	*35.4*	*33.4*
^{3}**M** + CH_4	*0.0*	*0.0*	*0.0*	*0.0*	*0.0*	*0.0*	*0.0*	*0.0*
M(CH_4)	*86.7*	*80.5*	*65.5*	*64.9*	*21.9*	*13.4*	*9.7*	*4.5*
M-MECP	*91.0*	85.7	*74.6*	76.7	29.6	24.4	*27.0*	25.2
M-TS$_{exch}$	*86.9*	81.1	*66.2*	66.4	23.4	15.8	*14.9*	10.8
M-TS$_{ins}$	*117.7*	108.2	*75.3*	72.0	49.3	40.0	*14.1*	7.8
M(H)(Me)	*40.8*	*34.2*	*-46.0*	*-45.0*	*–35.3*	*–41.8*	*–121.9*	*–123.3*

[a]Values in italics are taken from our previous contribution.[17]

Table 3. Energies (kJ mol^{-1}) relative to ^{3}**M**+CH_4 of various points on the relevant singlet and triplet potential energy surfaces for the **a-H$_2$Si-M** and **a-Me$_2$Si-M*** (M = Mo, W) metallocenes.

	M = **a-H$_2$Si-Mo** 6-31G**	M = **a-H$_2$Si-W** 6-31G**	M = **a-Me$_2$Si-Mo*** 6-31G**	M = **a-Me$_2$Si-W*** 6-31G**
^{1}**M** + CH_4	53.8	47.5	52.4	55.9
^{3}**M** + CH_4	0.0	0.0	0.0	0.0
M(CH_4)	36.8	24.2	41.4	37.4
M-MECP	43.2	39.1	46.6	49.2
M-TS$_{exch}$	40.4	33.5	44.1	44.0
M-TS$_{ins}$	62.5	28.6	64.3	39.2
M(H)(Me)	-13.2	-92.7	-17.1	-90.1

We shall discuss here only the relevant new points. For the more basic features of this system, we refer the reader to our previous contribution.[17] The relative energies at the two computational levels are in relatively good agreement within the singlet state. The 6-31G** basis set leads to somewhat lower triplet-singlet gaps for the 16-electron Mo systems, whereas nearly identical gaps are found at the two levels for the two W systems. The 6-31G** calculations lead, for all systems, to significantly lower **M-TS$_{ins}$** energies relative to the **M(CH$_4$)** complex, whereas the relative energy of the **M-MECP** is less affected. We shall provide a more detailed discussion of the relative energetics and geometries only on the basis of the 6-31G** results. These are given in Figure 2 and Figure 3. However, the considerations would be the same on the basis of the LANL2DZ results.

<Figure 2 and Figure 3>

For all systems, **M-TS$_{exch}$** is very low, leading to fast scrambling of the C-H bonds in the **M(CH$_4$)** intermediate. Only for the **a-W** system, the H exchange barrier is *higher* than the insertion barrier (6.4 vs. 3.3 kJ mol^{-1}), but scrambling is still favorable relative to CH_4 dissociation, as experimentally verified for the $Me_2C(C_5H_4)_2W$ system.[12] As we will discuss further on, this is concordant in terms of the high barrier induced by the **M-MECP**. The **M-TS$_{exch}$** geometry is in all cases symmetrical with identical M-H distances and a planar MH_2C arrangement with overall C_{2v} symmetry, in agreement with a previous report.[15]

For the **Cp$_2$M** systems (Figure 2), the qualitative picture remains the same as previously shown on the basis of the LANL2DZ calculations. For the Mo system, the oxidative addition barrier (TS) is much higher than the **M-MECP** (27.7 *vs.* 5.2 kJ mol^{-1}, relative to the **M(CH$_4$)** intermediate). For the W system, the **M-TS$_{ins}$** is slightly lower than the **M-MECP** (7.1 *vs.* 11.8 kJ mol^{-1}), whereas these two energies are closer at the LANL2DZ level. Experimentally,

H exchange and CH_4 elimination were found to be competitive, the H exchange barrier being slightly lower.[9] No experimental data is available to compare with for the Mo system. For the *ansa* systems (Figure 3), the CH_4 elimination is again more favorable than the oxidative addition for Mo, whereas oxidative addition is now strongly preferred for W. This picture is in qualitative agreement with the experimental observation of H scrambling processes for $Me_2C(C_5H_4)_2W(H)(CH_3)$, whereas no methane elimination occurs under the same conditions.[12]

2. a-H_2Si-M and a-Me_2Si-M* systems

The calculations on these two systems were only carried out at the B3LYP/6-31G** level. The energy results are reported in Table 3, while selected geometrical parameters are given in Figure 4 and Figure 5 for the **a-H_2Si-M** and **a-Me_2Si-M*** systems, respectively, together with a representation of the reaction coordinates for the reductive elimination and dissociation processes. Qualitatively, the picture does not differ too much from that of the **a-M** system for either metal.

Both silylene *ansa* systems display similar energetics to the corresponding **a-M** system for the reductive elimination step leading to the methane σ-complex, but greater energy gains upon methane dissociation. This fact can be related to the greater facility, for the silylene systems, to better relax the metallocene scaffold, because of the greater size of the silicon atom. This is particularly notable in the triplet state, because this benefits more than the singlet, from the energetic point of view, from a parallel geometry. The **a-M** system, on the other hand, is constrained by the smaller C atom to remain in a more strained, and therefore less energetically favorable geometry. The **M-TS$_{exch}$** energy is lower than the **M-TS$_{ins}$** energy for the two Mo systems and higher for the two W systems. In all cases, however, it is

lower than the **M-MECP** energy. This is in agreement with the occurrence of H scrambling processes between the hydride and the methyl ligands for the W system.

<Figure 4 and Figure 5>

3. Comparison of energies and geometries for the MECP and insertion TS

A full comparison of the four systems leads to a satisfactory rationalization of the relative barriers on the basis of Hammond's postulate concerning the relation between exothermicity and barrier height. The metal insertion into the C–H bond (C–H oxidative addition), starting from the **M(CH$_4$)** intermediate, has a smaller barrier for the group of W metallocenes (1.8-7.1 kJ mol^{-1} range), for which the process is more exothermic, and a greater one for the Mo group (22.9-27.7 kJ mol^{-1} range), for which the thermodynamics is less favourable. Within each group, the **M-TS$_{ins}$** barrier follows approximately the expected trend: for the W group, it decreases steadily from **Cp$_2$W** (7.1 kJ mol^{-1}) to **a-Me$_2$Si-W*** (1.8 kJ mol^{-1}) following the increase of energy gain, then it increases again for **a-W**. For the Mo group, it is highest for **Cp$_2$Mo**, which has the smallest energy gain, and lowest for **a-Me$_2$Si-Mo*** with the greatest energy gain. There is a small inversion of trend between the **a-H$_2$Si-Mo** and **a-Mo** systems.

The **M-TS$_{ins}$** geometry becomes more and more reactant-like (lower C–H, higher M–C and M-H distances) as the barrier decreases, as expected on the basis of Hammond's postulate. The trend is quite clear within the W group, the only inversion being witnessed for the W–C distance between **Cp$_2$W** and **a-H$_2$Si-W**. Within the Mo series, the C–H bond length follows the order of the energy gain (1.423 Å for **Cp$_2$Mo** > 1.414 Å for **a-H$_2$Si-Mo** > 1.406 Å for **a-Mo** > 1.388 Å for **a-Me$_2$Si-Mo***), rather than the order of the insertion barriers. On the other hand, the Mo–C distance is unexpectedly longer for **Cp$_2$Mo-TS$_{ins}$** (2.427 Å), whereas

the Mo–H distance is anomalously long, relative to the rest of the series, in **a-Mo-TS$_{ins}$**. Overall, the energetic and structural trends are quite in line with expectations, on the basis of the oxidative addition thermodynamics and Hammond's postulate.

The same considerations hold true for the CH_4 dissociation process, which involves the spin inversion phenomenon. For any pair of metallocenes containing the same ligand, the process is slightly more exothermic for Mo and the dissociation barrier (determined by the spin inversion process) is correspondingly smaller. Within each group of metallocenes containing the same metal, the barrier steadily decreases with an increase of energy gain for the *ansa* systems in the order **a-M** > **a-H$_2$Si-M** > **a-Me$_2$Si-M*** (**W:** 20.7, 14.9 and 11.8 kJ mol^{-1} *vs.* 4.5, 24.2 and 37.4 kJ mol^{-1}; **Mo**: 11.0, 6.4 and 5.2 kJ mol^{-1} *vs.* 13.4, 36.8 and 41.4 kJ mol^{-1}). On going further to the **Cp$_2$M** system, at first sight surprisingly, the further increase in methane dissociation energy is not accompanied by a further decrease of dissociation barrier, which takes exactly the same values as for the corresponding **a-Me$_2$Si-M*** system for each metal. This is due to the fact that methane dissociation is anomalously exothermic for this system, due to the relaxation energy associated with moving the two Cp rings parallel. In the MECP region, the presence of the methane molecule prevents both singlet and triplet states from adopting this parallel configuration, so that the local slope and curvature of the potential energy surfaces resemble those for the constrained C and Si ansa systems. The additional stabilization of the triplet only intervenes well beyond the MECP, and hence has no effect on the relative energy of the latter. The MECP geometry becomes correspondingly more reactant-like as the barrier decreases. Like for the oxidative addition TS examined above, there are a few exceptions, but the general trend is well respected. In particular, the trends of C–H, M–C and M–H distances are as expected within the *ansa*-W series. Particularly notable are the trends between the methylene and the silylene-bridged systems for both metals.

This comparison shows that Hammond's principle can successfully be applied as an approximate guide to predicting barrier heights and geometries for reaction steps involving a change in spin state. Although there are, *a priori*, no reasons why the principle should *not* apply in such cases, this does not appear to be a generally appreciated phenomenon. We previously discussed Hammond's postulate to rationalize trends in spin isomerization barriers for a series of *para*-substituted phenyl cations,[24] but there do not appear to have been other mentions in the context of spin-forbidden processes.

The exception mentioned above for the Cp_2M systems shows that, as for the more usual application to adiabatic reactions, the principle is only quantitatively reliable when all the potential energy surfaces for the set of analogous reactions have similar shapes. Where the endo- or exo-thermicity of one of the reactions considered is due to a feature of the potential energy surface which is not present in the other cases, and is not situated in the **TS_{ins}** or **MECP** region, deviations from the Hammond's principle predictions can be expected so some care should be taken when applying it to novel situations.

Conclusions

This study completes a previous one[17] in terms of the relative barriers to oxidative addition and elimination from metallocene σ-CH_4 complexes, and extends it to silylene-bridged *ansa* systems that have been the subject of recent experimental studies.[13] The comparison of the reaction barriers for the various systems considered in this study has shown that the relative barriers for both one-state and two-state processes can be generally related to the reaction energetics through the application of Hammond's postulate. Though minor differences can be related to changes in the ligand system (*ansa* vs. *non*-ansa, methylene- *vs.* silylene-bridged), a major effect on the energetic profile and on the related kinetic response is

due to the nature of the metal center. The calculation shows that the change of kinetic behavior for the same methane reductive elimination process from a hydridomethyl complex (*i.e.* from normal to inverse KIE from a Mo complex to the W analogue)[13] is regulated not only by changes in the energy of the reductive elimination TS, but also by changes, quantitatively as important, in the energy of the methane dissociation MECP.

Computational Methods

The bulk of the computations have been carried out using the well-established B3LYP hybrid density functional level of theory, as implemented in the Gaussian03[25] program package. The calculations were carried out using two different basis sets: (*i*) with the standard LANL2DZ basis set for all atoms, which includes an ECP on the W and Mo atoms; (*ii*) with a similar basis which includes polarization functions. Specifically, the LANL2DZ ECP and basis were retained on the metal atoms, but the standard 6-31G** basis was used on C and H (referred to as "6-31G**" henceforth). All structures were fully optimised, with the optimisation of the MECPs being carried out by a combination of Gaussian and the shell script/Fortran code of one of the authors.[26, 27] Geometry optimizations without symmetry constraints, backed up in several cases by computation of vibrational frequencies, showed all structures studied here to have at least C_S symmetry, with some belonging to higher point groups. Accordingly, the MECP optimizations were carried out within C_S symmetry. To further test the accuracy of the chosen method, we carried out additional calculations on the $[CH_2(C_5H_4)_2]W$ system only. Specifically, we characterized the singlet and triplet fragment, the σ-CH_4 intermediate and the methyl hydride product, using a larger basis set, with the SDD pseudopotential and associated basis set on W, and the 6-311++G** basis sets for C and H. Full geometry optimization was carried out with this basis set combinations and the B3LYP

functional used in the main body of the work, with additional single-point energies calculated using the same basis set, at the B3LYP geometries, with the B3PW91 and BP86 density functionals.

None of the reported energies include a correction for zero-point energy, as this is difficult to obtain at the MECPs. Nevertheless, frequencies have been calculated for all other stationary points, and used to identify them as minima or transition states.

Acknowledgments

RP thanks CINES and CICT (program CALMIP) for granting free CPU time. J.L.C.M. acknowledges support from Mexico's National Council for Science and Technology (CONACYT). JNH is an EPSRC Advanced Research Fellow.

References

[1] J. P. Collman, L. S. Hegedus, J. R. Norton, R. G. Finke, *Principles and Applications of Organotransition Metal Chemistry*, University Science Books, Mill Valley, CA, **1987**.
[2] R. H. Crabtree, *The Organometallic Chemistry of the Transition Metals*, 3rd ed., Wiley-Interscience, New York, **2001**.
[3] C. L. Hill, *Activation and Functionalization of Alkanes*, John Wiley and Sons, New York, **1989**.
[4] A. Shilov, G. B. Shul'pin, *Chem. Rev.* **1997**, *97*, 2879-2932.
[5] R. H. Crabtree, *J. Chem. Soc., Dalton Trans.* **2001**, 2951-2951.
[6] W. D. Jones, F. J. Feher, *Acc. Chem. Res.* **1989**, *22*, 91-100.
[7] B. A. Arndtsen, R. G. Bergman, T. A. Mobley, T. H. Peterson, *Acc. Chem. Res.* **1995**, *28*, 154-162.
[8] N. J. Cooper, M. L. H. Green, R. Mahtab, *J. Chem. Soc., Dalton Trans.* **1979**, 1557-1562.
[9] R. M. Bullock, C. E. L. Headford, K. M. Hennessy, S. E. Kegley, J. R. Norton, *J. Am. Chem. Soc.* **1989**, *111*, 3897-3908.
[10] G. Parkin, J. E. Bercaw, *Organometallics* **1989**, *8*, 1172-1179.
[11] L. Labella, A. Chernega, M. L. H. Green, *J. Chem. Soc., Dalton Trans.* **1995**, 395-402.
[12] A. Chernega, J. Cook, M. L. H. Green, L. Labella, S. J. Simpson, J. Souter, A. H. H. Stephens, *J. Chem. Soc., Dalton Trans.* **1997**, 3225-3243.
[13] D. Churchill, K. Janak, J. Wittenberg, G. Parkin, *J. Am. Chem. Soc.* **2003**, *125*, 1403-1420.
[14] P. A. Cox, P. Grebenik, R. N. Perutz, M. D. Robinson, R. Grinter, D. R. Stern, *Inorg. Chem.* **1983**, *22*, 3614-3620.

[15] J. C. Green, C. N. Jardine, *J. Chem. Soc., Dalton Trans.* **1998**, 1057-1061.
[16] M. D. Su, S. Y. Chu, *J. Phys. Chem. A* **2001**, *105*, 3591-3597.
[17] J. C. Green, J. N. Harvey, R. Poli, *J. Chem. Soc, Dalton Trans.* **2002**, 1861-1866.
[18] S. Shaik, D. Danovich, A. Fiedler, D. Schröder, H. Schwarz, *Helv. Chim. Acta* **1995**, *78*, 1393-1407.
[19] K. Janak, D. Churchill, G. Parkin, *Chem. Commun.* **2003**, 22-23.
[20] R. Poli, J. N. Harvey, *Chem. Soc. Rev* **2003**, *32*, 1-8.
[21] J. N. Harvey, *Struct. Bonding* **2004**, *112*, 151 - 184.
[22] J.-L. Carreón-Macedo, J. N. Harvey, *J. Am. Chem Soc.* **2004**, *126*, 5789-5797.
[23] R. Poli, I. Cacelli, *Eur. J. Inorg. Chem.* in press.
[24] M. Aschi, J. N. Harvey, *J. Chem. Soc., Perkin Trans. II* **1999**, 1059-1062.
[25] M. J. Frisch, G. W. Trucks, H. B. Schlegel, G. E. Scuseria, M. A. Robb, J. R. Cheeseman, J. Montgomery, J. A., T. Vreven, K. N. Kudin, J. C. Burant, J. M. Millam, S. S. Iyengar, J. Tomasi, V. Barone, B. Mennucci, M. Cossi, G. Scalmani, N. Rega, G. A. Petersson, H. Nakatsuji, M. Hada, M. Ehara, K. Toyota, R. Fukuda, J. Hasegawa, M. Ishida, T. Nakajima, Y. Honda, O. Kitao, H. Nakai, M. Klene, X. Li, J. E. Knox, H. P. Hratchian, J. B. Cross, C. Adamo, J. Jaramillo, R. Gomperts, R. E. Stratmann, O. Yazyev, A. J. Austin, R. Cammi, C. Pomelli, J. W. Ochterski, P. Y. Ayala, K. Morokuma, G. A. Voth, P. Salvador, J. J. Dannenberg, V. G. Zakrzewski, S. Dapprich, A. D. Daniels, M. C. Strain, O. Farkas, D. K. Malick, A. D. Rabuck, K. Raghavachari, J. B. Foresman, J. V. Ortiz, Q. Cui, A. G. Baboul, S. Clifford, J. Cioslowski, B. B. Stefanov, G. Liu, A. Liashenko, P. Piskorz, I. Komaromi, R. L. Martin, D. J. Fox, T. Keith, M. A. Al-Laham, C. Y. Peng, A. Nanayakkara, M. Challacombe, P. M. W. Gill, B. Johnson, W. Chen, M. W. Wong, C. Gonzalez, J. A. Pople, *Gaussian 03, Revision B.04*, Gaussian, Inc., Pittsburgh PA, **2003**.
[26] J. N. Harvey, M. Aschi, H. Schwarz, W. Koch, *Theor. Chem. Acc.* **1998**, *99*, 95-99.
[27] J. N. Harvey, M. Aschi, *Phys. Chem. Chem. Phys.* **1999**, *1*, 5555-5563.

Captions for Figures

Figure 1. Reaction coordinate leading from $Cp'_2M(H)(CH_3)$ to $Cp'_2M + CH_4$. (a) E(**M-TS$_{ins}$**) < E(**MECP**); (b) E(**M-TS$_{ins}$**) > E(**M-MECP**).

Figure 2. Reaction coordinate for the CH_4 oxidative addition to **Cp$_2$M**, with simplified views and selected bonding parameters (in Å) for the relevant optimized structures. The H atoms on the cyclopentadienyl rings have been omitted for clarity. All energies are at the B3LYP/6-31G** level.

Figure 3. Reaction coordinate for the CH_4 oxidative addition to **a-M**, with simplified views and selected bonding parameters (in Å) for the relevant optimized structures. The H atoms on the cyclopentadienyl rings have been omitted for clarity. All energies are at the B3LYP/6-31G** level.

Figure 4. Reaction coordinate for the CH_4 oxidative addition to **a-H$_2$Si-M**, with simplified views and selected bonding parameters (in Å) for the relevant optimized structures. The H atoms on the cyclopentadienyl rings have been omitted for clarity. All energies are at the B3LYP/6-31G** level.

Figure 5. Reaction coordinate for the CH_4 oxidative addition to **a-Me$_2$Si-M***, with simplified views and selected bonding parameters (in Å) for the relevant optimized structures. The H atoms on the silylene Me groups and the Me groups on the cyclopentadienyl rings have been omitted for clarity. All energies are at the B3LYP/6-31G** level.

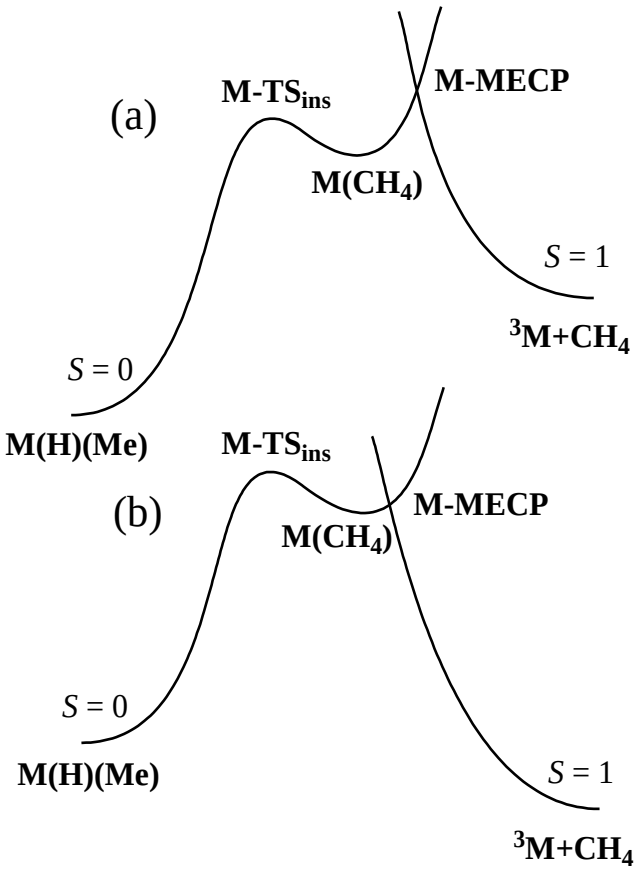

Figure 6. Reaction coordinate leading from Cp'$_2$M(H)(CH$_3$) to Cp'$_2$M + CH$_4$. (a) E(**M-TS$_{ins}$**) < E(**MECP**); (b) E(**M-TS$_{ins}$**) > E(**M-MECP**).

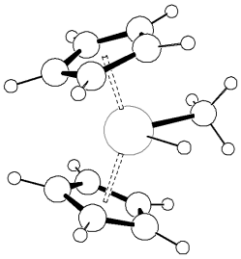

$Cp_2M(H)(CH_3)$ (M = Mo, W)

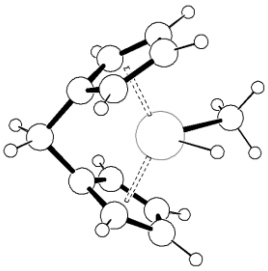

a-$M(H)(CH_3)$ (M = Mo, W)

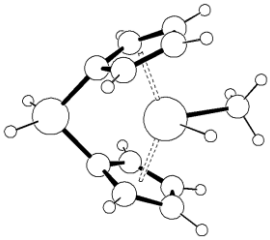

a-H_2Si-$M(H)(CH_3)$ (M = Mo, W)

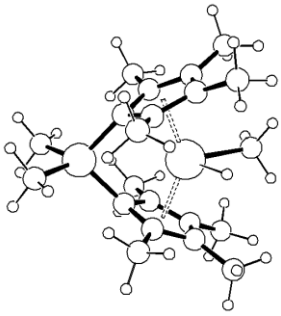

a-Me_2Si-M*$(H)(CH_3)$ (M = Mo, W)

Chart

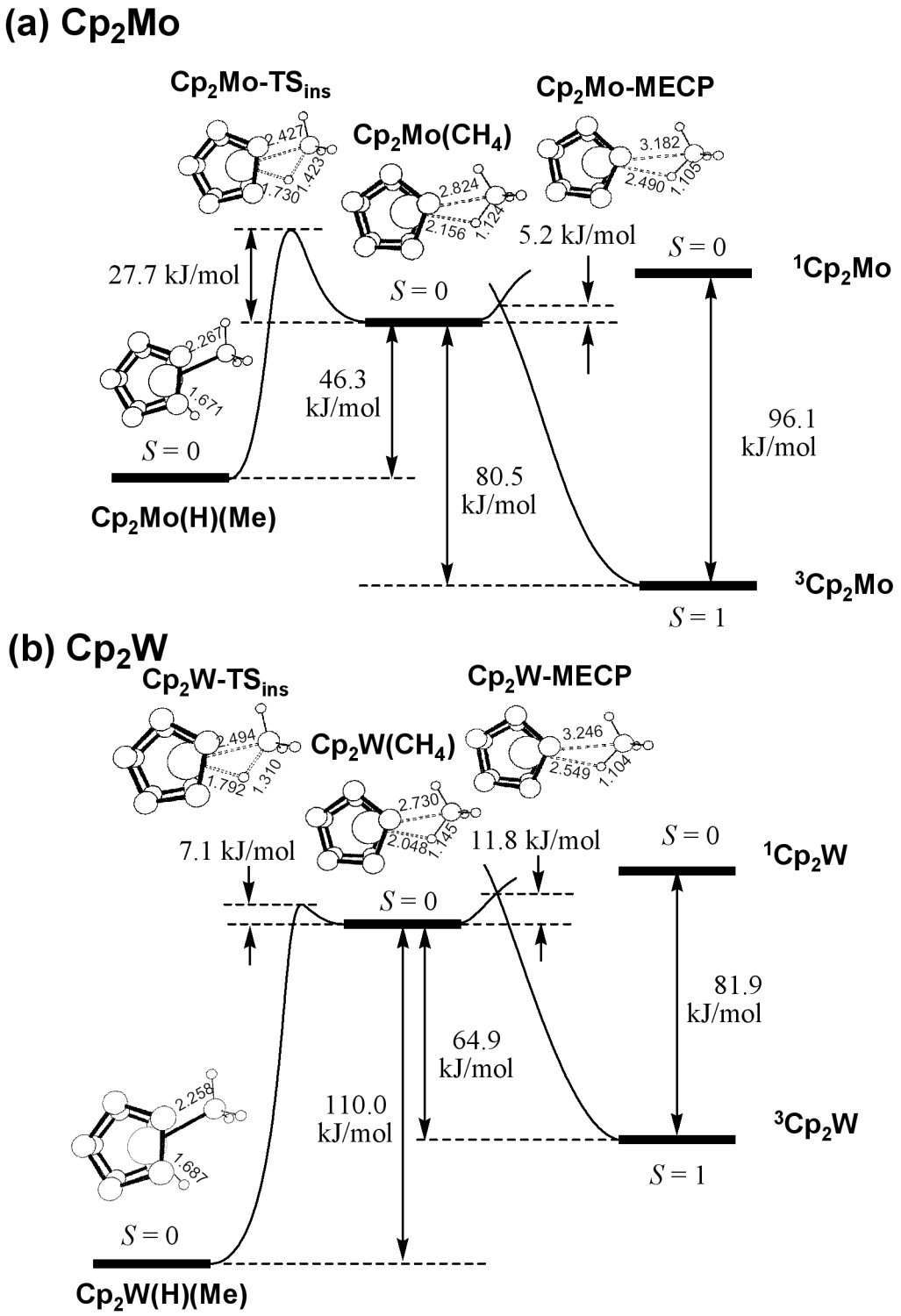

Figure 7. Reaction coordinate for the CH_4 oxidative addition to **Cp_2M**, with simplified views and selected bonding parameters (in Å) for the relevant optimized structures. The H atoms on the cyclopentadienyl rings have been omitted for clarity. All energies are at the B3LYP/6-31G** level.

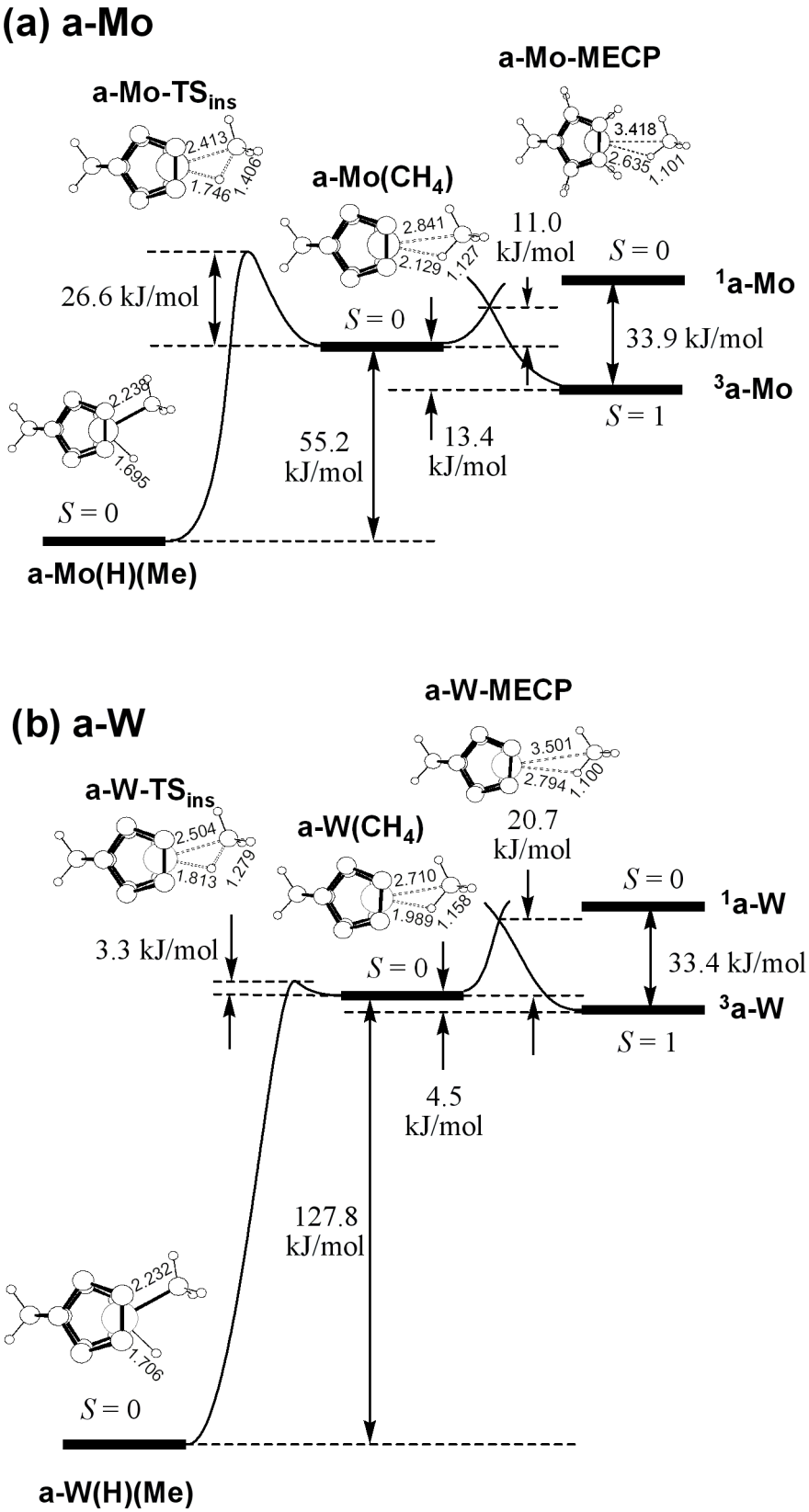

Figure 8. Reaction coordinate for the CH_4 oxidative addition to **a-M**, with simplified views and selected bonding parameters (in Å) for the relevant optimized structures. The H atoms on the cyclopentadienyl rings have been omitted for clarity. All energies are at the B3LYP/6-31G** level.

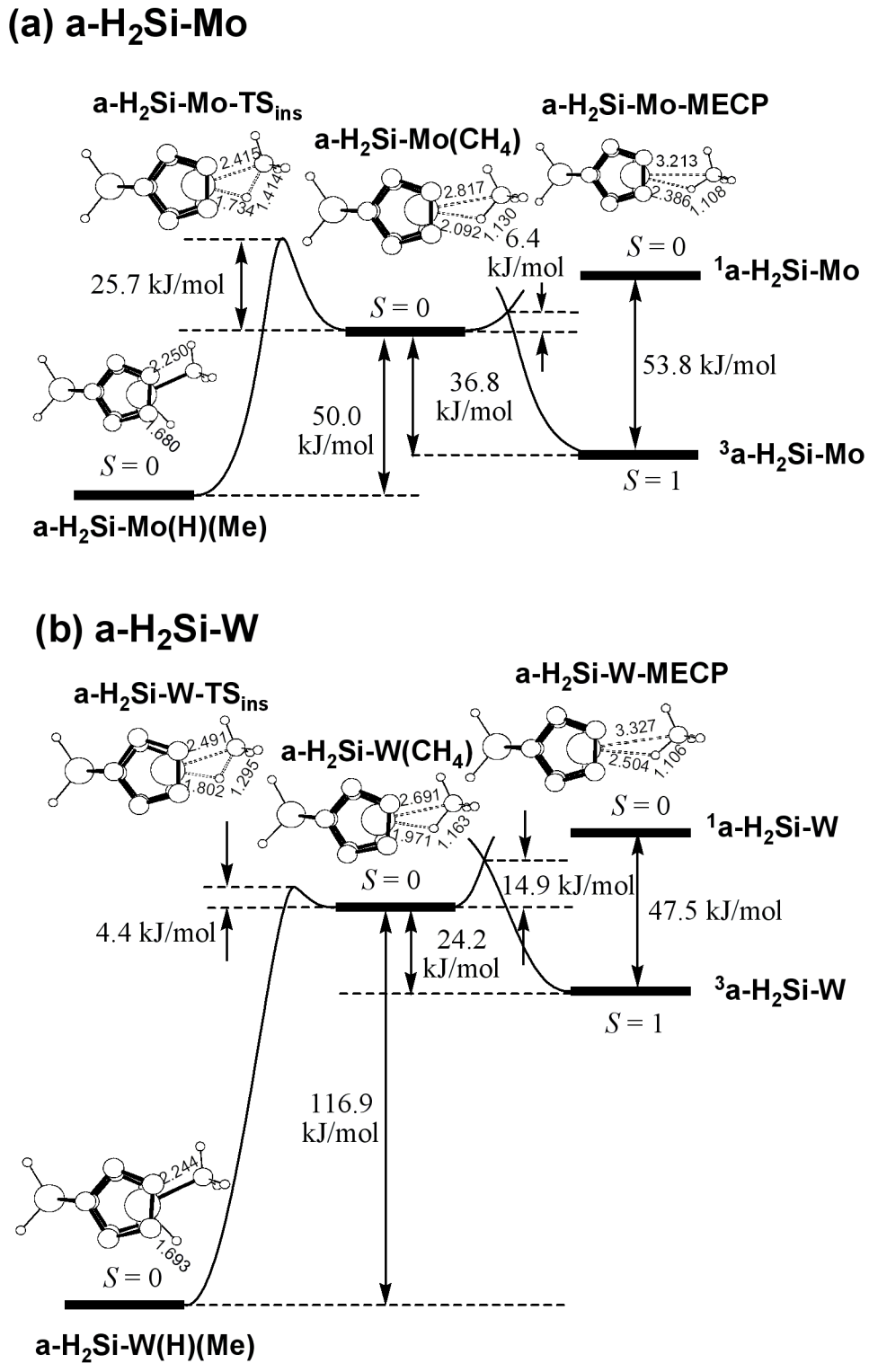

Figure 9. Reaction coordinate for the CH_4 oxidative addition to **a-H₂Si-M**, with simplified views and selected bonding parameters (in Å) for the relevant optimized structures. The H atoms on the cyclopentadienyl rings have been omitted for clarity. All energies are at the B3LYP/6-31G** level.

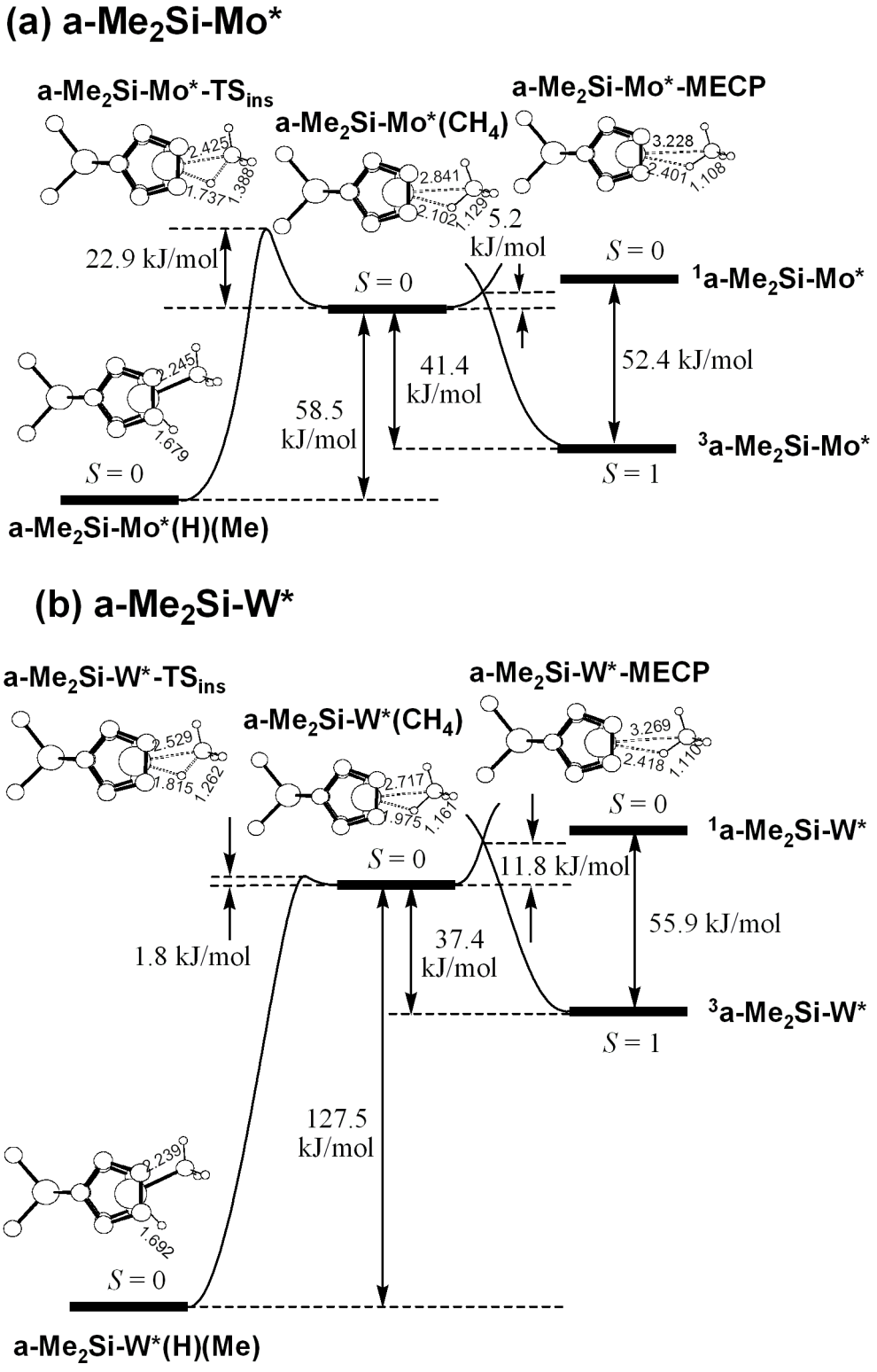

Figure 10. Reaction coordinate for the CH_4 oxidative addition to **a-Me$_2$Si-M***, with simplified views and selected bonding parameters (in Å) for the relevant optimized structures. The H atoms on the silylene Me groups and the Me groups on the cyclopentadienyl rings have been omitted for clarity. All energies are at the B3LYP/6-31G** level.

Table of Content Graphic